Chemistry–A European Journal
Research Article
doi.org/10.1002/chem.202203790
Chemistry Europe
European Chemical Societies Publishing
www.chemeurj.org

Morphology-Dependent Aggregation-Induced Emission of Janus Emulsion Surfactants

Pablo Simón Marqués,[a] Martyna Krajewska,[a, b] Bradley D. Frank,[a] Krystyna Prochaska,[b] and Lukas Zeininger*[a]

Abstract: We report a novel stimuli-responsive fluorescent material platform that relies on an evocation of aggregation-induced emission (AIE) from tetraphenylethylene (TPE)-based surfactants localized at one hemisphere of biphasic microscale Janus emulsion droplets. Dynamic alterations in the available interfacial area were evoked through surfactant-induced dynamic changes of the internal droplet morphology that can be modulated as a function of the balance of interfacial tensions of the droplet constituent phases. Thus, by analogy with a Langmuir–Blodgett trough that enables selective concentration of surfactants at a liquid–gas interface, we demonstrate here a method for controllable modulation of the available interfacial area of surfactant-functionalized liquid–liquid interfaces. We show that a morphology-dependent alteration of the interfacial area can be used to evoke an optical signal, by selectively assembling synthesized TPE-based surfactants on the respective droplet interfaces. A trigger-induced increase in the concentration of TPE-based surfactants at the liquid–liquid interfaces results in an evocation of aggregation-induced emission (AIE), inducing an up to 3.9-fold increase in the measured emission intensity of the droplets.

Introduction

Stimuli-sensitive fluorescent probes are central to many applications, including optics, information storage and processing, as well as transducers and signal amplifiers in diagnostic detection, screening, and sensing platforms.[1–3] Materials capable to dynamically and reversibly alter their fluorescence are particularly useful to convert physical or chemical stimuli into a readable optical signal and present advantages such as a facile and cost-effective implementation into automated analysis platforms.[4,5] The approach further provides the basis for real-time, dosimetric and multi-analyte sensing arrays, ensuring low cost and high sensitivity. Examples for the latter include the development of FRET-based small-molecule chemiluminescent probes,[6] identification of precise microbiological and biochemical constituents within widely employed enzyme-linked immunosorbent assays (ELISA),[7] as well as dyes that display a trigger-induced aggregation-induced emission (AIE) enhancement,[8,9] that is, a fluorescence intensification upon the formation of aggregates. Innovations in new functional stimuli-responsive fluorescent material platforms complement the development of microscopic imaging techniques and promise to expand the capabilities of present hardware in imaging, biosensing platforms, or data storage and processing, with the goal to drive down the cost and ensure broad implementation of these methods.[10]

In this context, biphasic microscale Janus emulsions have recently emerged as a versatile, inexpensive, and broadly programmable stimuli-responsive material platform.[11] Janus emulsions are comprised of kinetically stabilized droplets with two phase-separated liquid dispersed phases.[12] The morphology of Janus emulsions is exclusively dictated by the force balance of interfacial tensions acting at the various interfaces.[13] As a result, Janus droplets exhibit dynamic internal morphologies, and small variations in surfactant composition or effectiveness can transduce into significant changes in their internal geometry. This chemical–morphological coupling inside Janus emulsions, that is, the reversible tunability of their internal geometry as a function of their chemical environment has entailed a series of transformative application concepts, including their use as versatile refractory optical elements,[14–16] liquid templates for the generation of precision objects,[17–19] and as powerful sensors for a series of chemical and biological analytes.[20–25] Particularly the implementation of Janus emulsions as novel modular signal amplifiers in liquid biosensing platforms requires an efficient transduction of chemically-induced morphological transitions into a readable signal output. Thus far, a series of transduction paradigms have been developed to produce morphology-dependent changes in the

[a] Dr. P. S. Marqués, M. Krajewska, B. D. Frank, Dr. L. Zeininger
Department of Colloid Chemistry
Max Planck Institute of Colloids and Interfaces
Am Muehlenberg 1, 14476 Potsdam (Germany)
E-mail: lukas.zeininger@mpikg.mpg.de
Homepage: https://www.mpikg.mpg.de/6207047/responsive-soft-materials-interfaces

[b] M. Krajewska, Prof. Dr. K. Prochaska
Institute of Chemical Technology and Engineering
Poznan University of Technology
Berdychowo 4, 60-965, Poznan (Poland)

Supporting information for this article is available on the WWW under https://doi.org/10.1002/chem.202203790

optical characteristics of gravity-aligned Janus droplets. The latter include a morphology-dependent alteration of their refractive, reflective, or emissive properties, which typically are based on the refractive index contrast between the two constituent droplet phases.[26–28]

In order to improve broad applicability, advance the signal-to-noise ratio and to allow for the use of Janus emulsion optical elements in turbulent media as well, we communicate herein an alternative optical transduction mechanism that is not based on the intrinsic refractory optical properties of Janus emulsions. Based on the intrinsic feature of dynamically reconfigurable Janus emulsions to selectively hide and expand liquid–liquid interfaces, we anticipated that a selective concentration of chromophores at one of the interfaces of Janus emulsions results in a tunable emission intensity as a function of droplet morphology. More specifically, we opted for an assembly of tetraphenylethylene (TPE)-functionalized surfactants, which are reportedly known to undergo AIE (Figure 1). Thus, in analogy to a Langmuir–Blodgett trough, where surfactants can be concentrated at a liquid–gas interface, we herein report a method to controllably increase the concentration of AIE surfactants at the liquid–liquid interfaces of Janus emulsions thus causing a trigger-induced evocation of an optical read-out signal. The latter is central to many applications of Janus emulsions, particularly their use as transducer and signal amplifier in liquid sensing platforms.

Results and Discussion

TPE is a fluorescent molecule with widespread use due to its synthetic accessibility and remarkable AIE-properties.[29] Typically, planar luminophoric molecules tend to aggregate due to the strong π-π stacking interactions between the aromatic rings, which is commonly followed by a decrease of the quantum yield. However, AIE molecules behave oppositely, with their light emissions turned "on" upon aggregate formation, due to the restriction of intramolecular rotation (RIR) in the aggregated state.[30] This AIE phenomenon provides an exciting avenue to impart materials with the capability to release a stimuli-triggered optical signal, a concept that has been previously elegantly designed and used in a variety of applications, including in optical sensors[31] and organic electronics.[32] To sensitize Janus droplets with TPE chromophores, we first synthesized amphiphilic TPE-based surfactants. We aimed at three different surfactants, distinguished by their hydrophilic portions (sodium sulfonate **5**, ammonium bromide **6**, and poly(acrylic acid) (PAA) **7**), which were selected to study the different behavior of anionic, cationic and polymer surfactants.

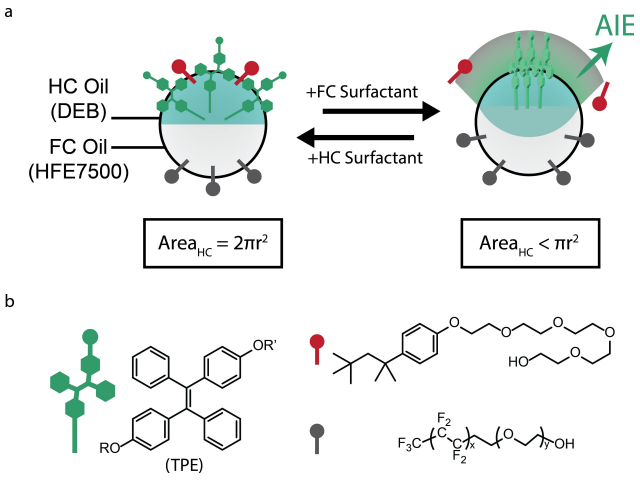

Figure 1. Conceptual sketch of an evocation of an AIE of TPE-based surfactants by reversibly shrinking and expanding the hydrocarbon–water interface of reconfigurable Janus emulsions. HC = hydrocarbon; FC = fluorocarbon.

Following a divergent synthetic strategy, desymmetrization was used to prepare all three surfactants from common intermediates (Figure 2). Starting from dihydroxy TPE, we first synthesized mono-alkyl substituted **2** by nucleophilic substitution of one alcohol functionality. The anionic sodium sulfonate surfactant **5** (TPE-SS) was then obtained after trapping 1,4-butanesultone under basic conditions. After converting compound **2** to intermediate **3**, stable TPE-derivative **6** (TPE-TAB) was obtained by quarternization of trimethylamine with the bromine-derivative **3**. Following a conversion of **3** into the azide **4**, a click-type azide–nitrile cycloaddition with a nitrile-terminated polystyrene-polyacrylic acid block-copolymer yielded the polymeric surfactant **7** (TPE-BCP). While the anionic surfactant TPE-SS was water-soluble, the cationic TPE-TAB and polymeric surfactant TPE-BCP displayed solubility in organic media.

We next investigated the AIE characteristics of the three surfactants. Upon excitation at 365 nm, TPE-SS, TPE-TAB, and TPE-BCP displayed an emission-structured band at $\lambda = 480$ nm in aqueous media. The water solvation of the surfactants prompted the formation of TPE aggregates, resulting in the restriction of the phenyl rotation and therefore a pronounced photoluminescence (PL). Small amounts of organic solvents could release the molecular rotation of AIE compounds, reducing exponentially the PL band, which we monitored by titration of the aqueous mixture with MeCN and THF. In these experiments, all three amphiphiles displayed a PL reduction greater than twofold compared to the initial intensity (Figure 3).

The three synthesized compounds TPE-SS, TPE-TAB, and TPE-BCP were capable of successfully stabilize oil-in-water emulsions. Following a literature procedure to determine the critical micelle concentration (CMC) of the surfactants, we measured the PL intensity at different concentrations (Figure S7 in the Supporting Information).[33,34] Due to the higher freedom of the phenyl ring rotation within micelles, the trend of fluorescence intensity with concentration varies on the formation of micelles. The CMC of the three TPE derivatives were determined to be 26 μM (0.016 wt.%) for TPE-SS, 37 μM for TPE-TAB (0.025 wt.%), and 0.016 wt.% for the polymeric surfactant TPE-BCP. As revealed by force tensiometry, all three compounds lowered the interfacial tension between water and the hydrocarbon oil diethylbenzene. TPE-TAB proved to be most effective (4.54 mN m^{-1}), when compared to TPE-SS (23.55 mN·m^{-1}), or TPE-BCP (22.05 mN·m^{-1}) at equal concentrations of the surfac-

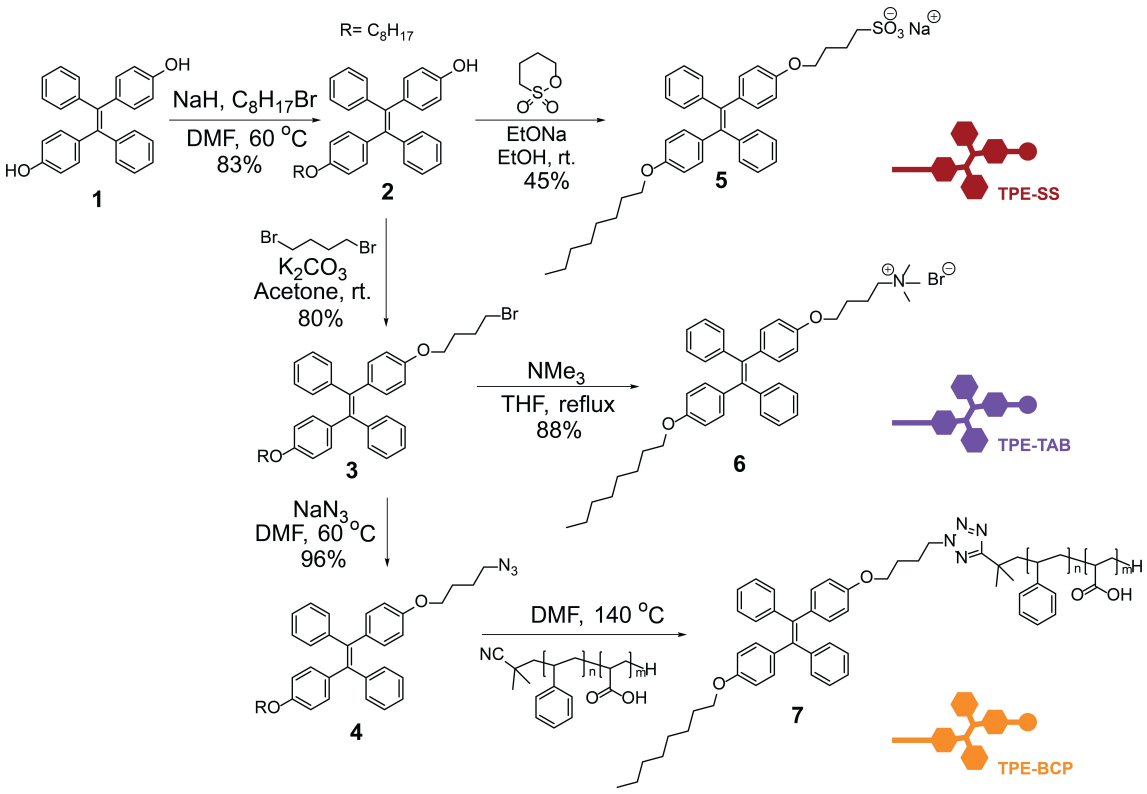

Figure 2. Synthetic routes towards the amphiphilic TPE compounds **5** (TPE-SS), **6** (TPE-TAB), and **7** (TPE-BCP).

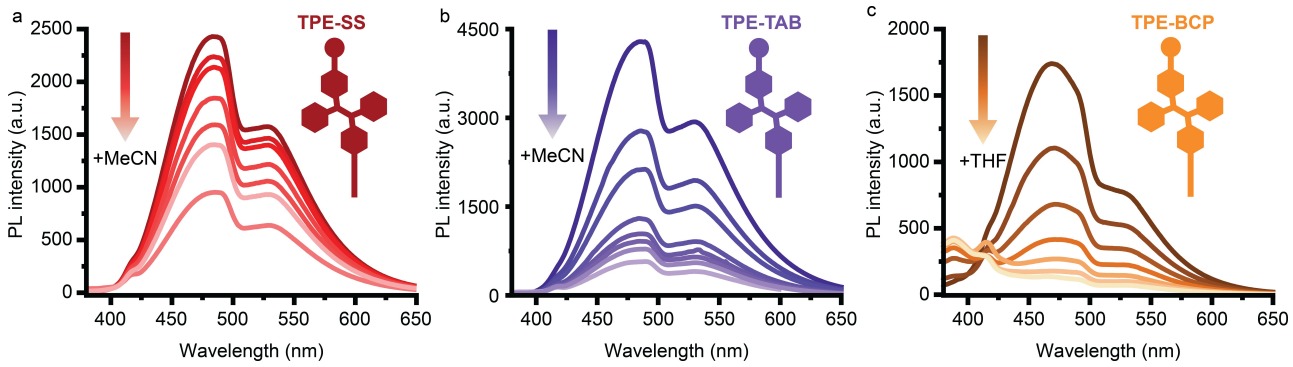

Figure 3. Emission spectra of TPE-SS (red), TPE-TAB (blue), and TPE-BCP (orange) in water; $c = 10^{-6}$ M; $V = 2$ mL; $\lambda_{ex} = 365$ nm. Subsequent addition of small aliquots (10 μL) of MeCN or THF reduced the PL intensity exponentially.

tants (0.1 wt.%; Figure 4a), which also prompt the most pronounced AIE behavior of the ammonium derivative (Figure 3). Next, we set out to selectively sensitize one interface of biphasic Janus emulsions with the newly prepared surfactants. To this end, we prepared droplets comprised of a phase-separated mixture of a hydrocarbon (DEB) and a fluorocarbon (HFE-7500) oil inside a surfactant-containing aqueous continuous phase, using an established thermal phase separation approach.[12] The morphology of the biphasic Janus droplets is exclusively controlled by the force balance of interfacial tensions acting at the various interfaces. Consequently, stabilization of Janus emulsions using both hydrocarbon surfactants, Triton X and one of the synthesized AIE surfactants, that is, TPE-SS, TPE-TAB, or TPE-BCP, in combination with a fluorocarbon surfactant, such as Zonyl, yielded droplets in Janus morphologies.

To ensure selective assembly and partitioning of the surfactants to the hydrocarbon water interface of Janus emulsions we investigated the surfactant concentration dependent variation of Janus droplet morphologies (Figure S8). At low concentrations of the synthesized surfactants, the droplets persisted in almost "closed-up" Janus conformations, quantified by low triple-phase contact angles (Scheme S1). An increase of the TPE surfactant concentrations then resulted in an alteration

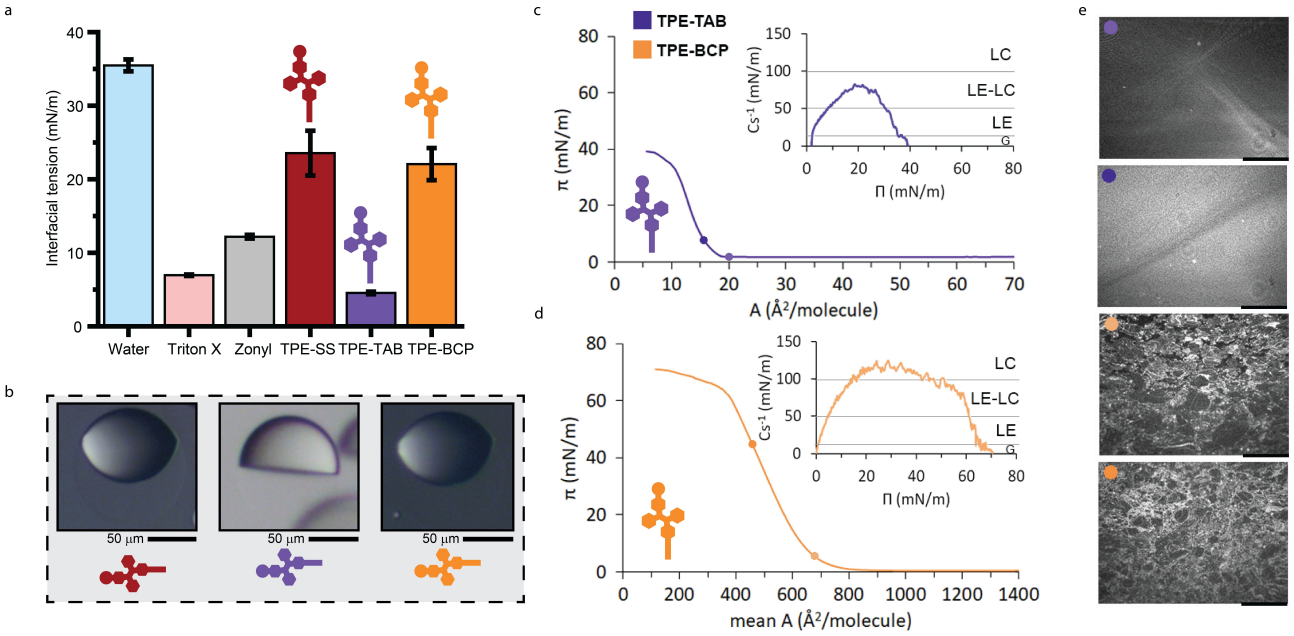

Figure 4. a) Interfacial tension between DEB and water with and without the addition of 0.1 wt.% of different surfactants. b) Side-view micrographs of Janus droplets stabilized by Zonyl and Triton X (1.0 wt%), and 0.2 wt.% of the synthesized TPE surfactants **5**, **6** and **7** displaying their different effects on the internal Janus droplet morphology. π-*A* isotherms of c) TPE-TAB and d) TPE-BCP as measured using the Langmuir technique; insets display the compression modulus (Cs^{-1}) with the ranges assigned to the state of the monolayer. e) Brewster angle micrographs recorded during monolayer compression; colored dots represents the surfactant type and surface pressure at which the images were taken. Scale bar: 1 mm, LC: liquid condensed state, LC–LE: liquid condensed–liquid expanded state, LE: liquid expanded state, G: gaseous state.

of the droplet geometry towards more "opened-up" Janus morphologies. The latter demonstrated the lowering of the interfacial tension at the hydrocarbon–water interface of the droplets and thus a preferential assembly of the synthesized surfactants at the latter (Figure 4b). The latter was most pronounced for droplets stabilized by TPE-TAB ($\Theta = 79.8°$), which indicated the highest surfactant effectiveness of the latter when compared to TPE-SS ($\Theta = 31.7°$) and TPE-BCP ($\Theta = 33.8°$) at equal concentrations (0.1 wt.%), reflecting our findings from the interfacial tension measurements.

To explore localized compression of surfactant monolayers at interfaces, we used the Langmuir technique to analyze π–*A* isotherms of the TPE amphiphiles (Figure 4c and d). To this end, organo-soluble compounds TPE-TAB and TPE-BCP were dissolved in ethanol and chloroform respectively at a concentration of 1 mg/mL, and the spreading solutions gently placed onto a water subphase. After evaporation of the volatile solvent, the surface pressure (π) as a function of available area per molecule (*A*), was recorded with compression until the monolayers collapsed (for the macromolecular derivative TPE-BCP, the mean area was used). In these experiments, both TPE-TAB and TPE-BCP formed stable and insoluble monolayers at the interface. While the TPE-TAB monolayer was compressible to a low area per molecule, with collapse occurring at $\pi = 37$ mN/m, TPE-BCP exhibited a relatively high limiting area of 700 Å^2 and collapsed at $\pi = 65$ mN/m.

The compressibility modulus (Cs^{-1}) proved that according to the classification of Davies and Rideal,[35] TPE-BCP displayed a liquid condensed state, while TPE-TAB at its maximal compression, was at an intermediate liquid expanded–liquid condensed state. Notably, when compressed to 50 mN/m the TPE-BCP monolayer became turbid, and its structure was visible by eye (Figure S9). We attributed this abnormal behavior to the polymeric chain dehydration at severe monolayer compression observable in Brewster angle micrographs of TPE-BCP, where the dense lattice increases in density with surface pressure (Figure 4e). The high compressibility of the TPE-BCP monolayer and the lattice structure indicated an increased interfacial localization and low surfactant exchange dynamics at the interface.

Motivated by these findings, we next set out to investigate the evocation of AIE of the surfactants at the interface of Janus emulsion droplets. Based on the intrinsic ability of reconfigurable droplets to reversibly hide or expose interfaces, we investigated the morphology-dependent emission intensity of Janus droplets stabilized by the different TPE-based surfactants. To this end, we prepared Janus droplets stabilized by a mixture of one of the AIE-surfactants (TPE-SS, TPE-TAB, or TPE-BCP at 0.1 wt%) in combination with both a fluorocarbon surfactant Zonyl (0.5 wt%) and the commercial hydrocarbon surfactant Triton X (1.5 wt%). The starting morphology of all droplets was set to the perfect Janus shape, that is, a droplet with two perfect hemispheres, as characterized by the triple phase contact angle of $\Theta = 90°$. Stepwise addition of Zonyl then resulted in a closing-up of the droplets towards lower contact angles $\Theta < 90°$. We simultaneously monitored the droplets' emission intensity while decreasing the hydrocarbon–water interfacial area (Figure 5a). Here, we initially observed only

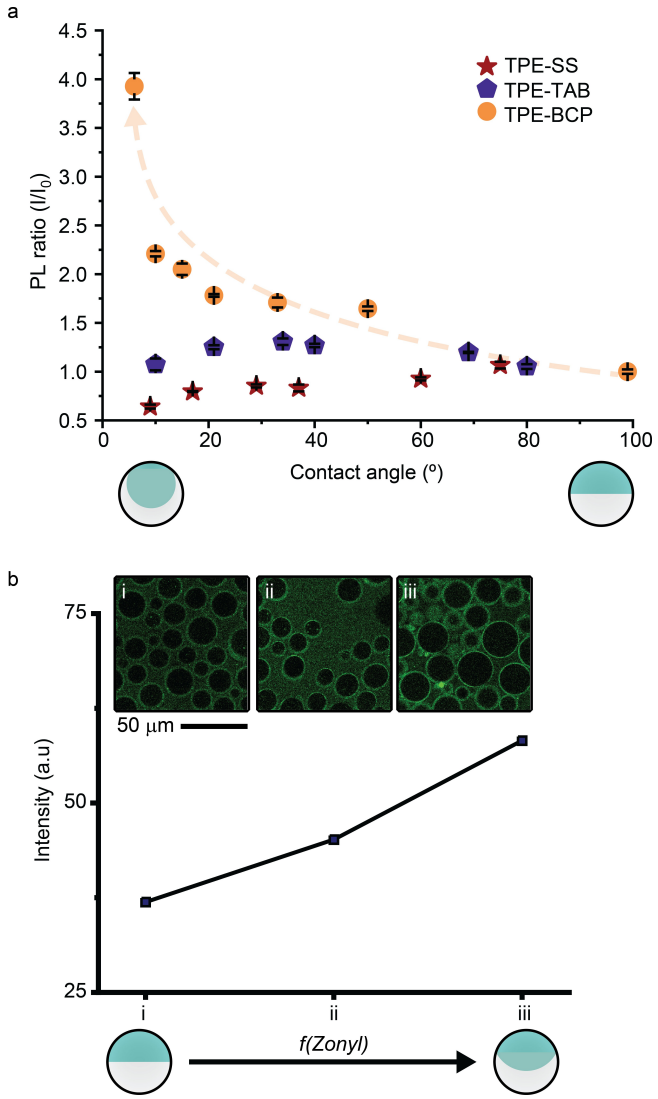

Figure 5. a) Correlation of the relative emission (PL ratio) to the Janus droplet contact angle. b) Fluorescence confocal micrographs of TPE-BCP after two subsequent addition of Zonyl (10 μL; 10.0 wt% in water).

marginal PL intensity variations for the anionic surfactant TPE-SS, until at contact angles of $\Theta = 50°$ and lower, a drop in emission intensity was observed. This observation could be explained by its water solubility, the pronounced exchange dynamics, and lower surfactant effectiveness as compared to Triton X and Zonyl, which consequently resulted in removal of the surfactants from the interface upon droplet morphological reconfiguration.

In contrast, the morphology-dependent recording of Janus emulsions stabilized by the surfactant TPE-TAB revealed an increase of the emission intensity upon compression at the liquid–liquid interface (Figure S11). This could be attributed to the stronger surfactant effectiveness of TPE-TAB compared to Triton X, and thus initial removal of the latter. Due to the organo-solubility of the surfactant, a further increase in Zonyl concentration, however, resulted in a further closing-up of the Janus droplet morphologies and thus again, a drop in PL intensity upon approaching droplet contact angles of $\Theta = 30°$ an lower.

Whereas for the molecular surfactants TPE-SS and TPE-TAB the compressibility at the dynamic interface of Janus emulsions did not suffice to evoke a pronounced AIE intensity, a strong increase in PL intensity upon lowering the hydrocarbon-water interfacial area could be observed for of the polymeric surfactant TPE-BCP. Due to the low surfactant exchange dynamics, the co-polymeric surfactant TPE-BCP displayed an up to 3.9-fold increase in fluorescence intensity as the hydrocarbon-water interfacial area was reduced. These results were corroborated by Brewster-angle micrographs of TPE-BCP on the Langmuir trough (Figure 4e). Here, monolayers of TPE-BCP were stable also after monolayer expansion, supporting our findings on a high immobilization and aggregation of TPE-BCP upon compression at the interface of Janus emulsions, which triggered the enhanced emission. AIE of TPE-BCP surfactants at Janus emulsion interfaces could further be confirmed using confocal fluorescence micrographs (Figure 5b). An in-situ observation of the fluorescence response of TPE-BCP functionalized Janus droplets confirmed the selective localization of the AIE-surfactants at the hydrocarbon-water interface of the droplets and the increase in emission intensity with lowered interfacial area of the latter.

Conclusion

In summary, three TPE-based amphiphiles have been synthesized to study surfactant partitioning to an interface, immobilization at that interface, and ultimately the evocation of AIE at Janus emulsion interfaces. Each molecule (TPE-SS, TPE-TAB, and TPE-BCP) displayed induced emission in solution due to intermolecular aggregation, as well as surfactant properties. We demonstrated that by using the polymeric surfactant TPE-BCP an up to 3.9-fold increase in emission intensity could be evoked upon dynamically reducing the area of the functionalized liquid–liquid interface of Janus emulsions. A significantly lower performance of the molecular surfactants TPE-SS and TPE-TAB in this context could be explained by lower interfacial activity and higher exchange dynamics, as confirmed by experiments using the Langmuir technique. The excellent morphology-dependent emission response of TPE-BCP-functionalized Janus droplets offers an opportunity for the characterization of surfactant partitioning to interfaces, as well as for a straightforward inexpensive, selective, and sensitive transduction of chemical signals within new and improved Janus emulsion-based liquid chemo- and biosensing platforms.

Experimental Section

Chemicals: All reagents were analytical grade and used as received without further purification. AIE-surfactants **1**, **2**, **3**, **5** and **6** were synthesized following procedures previously reported in the literature.[33,34] TPE derivative **4** was synthesized according to the following procedure: A round-bottom flask was charged with **3** (180 mg, 0.29 mmol) and NaN_3 (36 mg, 0.59 mmol) and the mixture

dissolved in DMF (3 mL). The reaction was stirred overnight at 80 °C and cooled down before drying under vacuum. The crude was purified by column chromatography using silica-gel (eluent: hexanes/dichloromethane) to afford a yellow sticky solid (160 mg, 95% yield). ^{1}H NMR (400 MHz, $CDCl_3$): $\delta = 7.36–7.30$ (m, 1H), 7.24–6.83 (m, 13H), 6.67–6.58 (m, 4H), 4.06–3.80 (m, 4H), 3.41–3.30 (m, 2H), 1.77 (m, 6H), 1.27 (m, 9H), 0.88 (m, 4H). HRMS (TOF-ES+): calculated for $C_{38}H_{43}N_3O_2$ 573.3350, found 573.3376. The TPE surfactant **7** was obtained by post-functionalization of commercially available Polystyrene-block-poly(acrylic acid) block-co-polymer. For the synthesis of **7** a Schlenk tube was charged with **4** (40 mg, 0.07 mmol) and 2 g of PS-b-PAA under inert N_2 atmosphere, and the solids were dissolved in 5 mL DMF. The mixture was heated to 160 °C overnight until TLC revealed consumption of **4**. The polymer was subsequently precipitated from ethanol, then filtrated and washed with methanol. Successful post-functionalization was confirmed by fluorescence and NMR spectroscopy (Figures S6 and S7). All TPE derivatives were comprised of a mixture of cis and trans isomers. In the manuscript the trans conformation is depicted only for simplification. Commercial surfactants and droplet solvents were used as received without further purification. DI water was used as the emulsion continuous phase and ultrapure water (pH 6.25, 18 MΩ·cm, 71.98 ± 0.01 mN/m) as the subphase in Langmuir experiments.

Complex droplet generation: Biphasic Janus emulsion droplets were generated employing an established thermal phase separation procedure.[12] The oil phase consisted of a 1:1 mixture of the hydrocarbon oil diethylbenzene and fluorocarbon oil HFE7500. Depending on their solubility, synthesized AIE surfactants were solubilized in the surfactant-containing aqueous continuous phase (**5**) or in the diethylbenzene phase (**6** and **7**) pre-emulsification. For emulsification, 100 μL of a 1:1 DEB-HFE7500 mixture was heated above its upper critical solution temperature (UCST) of 47 °C, and subsequently added to 1 mL of the pre-heated aqueous surfactant solution before emulsification by vortex mixing (10 s, Vortex Genie 2, scientific industries). The prepared complex emulsions were allowed to cool back to room temperature to induce phase separation of the two oils prior to imaging.

Optical and fluorescence microscopy experiments: Inverted optical microscopy was performed with a Bresser IVM 401 microscope. Prior to imaging, the emulsions were deposited into an Invitrogen Attofluor Cell Chamber from Thermo-Fisher Scientific. For horizontal imaging of emulsion droplets, we used a custom designed side-view setup which was equipped with a variable zoom, composed of two tube 200 mm tube lenses and Olympus planar optical microscopy lenses. The apparatus was connected to an area scan CCD camera from HIKVision. For imaging, emulsion droplets were trapped between a cavity well slide and coverslip to enable the droplets to be imaged vertically. The concave well of the slide allows free suspension of the droplets and the images were taken after the droplets settled into their gravitational alignment. Photoluminescent spectra and intensity were measured on a Jasco FP-8300 instrument. To monitor the correlation between the PL and the Janus droplet morphology, emulsions were transferred to a quartz cuvette and the emission intensity measured using the spectrofluorometer. Confocal microscopy was performed with a Leica SP8 confocal microscope with a 10 x lens, scanning 1024×1024 pixels at 200 Hz, 446 nm argon laser applied, and emission detection at 512 nm. Due to density difference, droplets align with gravity, with the denser fluorocarbon phase at the bottom. To monitor the surfactant PL, a sample containing complex emulsions stabilized by TPE-BCP (0.1 wt%), Zonyl (0.5 wt%) and Triton X (1.5 wt%) was subsequently titrated with Zonyl (10 μL; 10.0 wt% in water). After each addition, a small aliquot of the droplets sample was deposited between two round coverslips smoothly, to avoid droplet coalescence and analyzed under the confocal microscope.

Langmuir experiments: π–A isotherms were recorded by using a Teflon trough with 273 cm^2 surface area. The trough by KSV NIMA (Finland) was equipped with two movable barriers to compress and expand monolayers at a speed equal to 10 mm/min. During the experiments, a Julabo F12 circulator maintained the subphase temperature at 25 ± 0.1 °C. Every isotherm was conducted at least 5 times to confirm the reproducibility of the results. Surfactant TPE-TAB was dissolved in ethanol and TPE-BCP in chloroform (as well as in ethanol/chloroform 1:1) to the concentration of 1 mg/mL and gently placed the spreading solutions onto the water subphase. Surfactant solutions were carefully applied to the water subphase using the Hamilton microsyringe. After 10 min (for the volatile solvent evaporation), the monolayer was compressed until it collapsed. The surface pressure (π) and the area per molecule/mean area per molecule (A) were recorded to obtain π-A isotherms. The compression modulus Cs^{-1} was calculated based on the π–*A* isotherm data. Brewster Angle Microscopy (BAM) images were obtained using a MicroBAM by KSV NIMA during recording the π-A isotherms.

Acknowledgements

The authors acknowledge funding through the "Experiment!" program of the Volkswagen (VW) foundation and through the Emmy-Noether program of the German Research Foundation under grant no. ZE1121/3-1 and financial support from the Max Planck Society. This work was also supported by the Ministry of Science and Education (Poland). Open Access funding enabled and organized by Projekt DEAL.

Conflict of Interest

The authors declare no conflict of interest.

Data Availability Statement

The data that support the findings of this study are available in the supplementary material of this article.

Keywords: aggregation-induced emission · fluorescent probes · Janus emulsions · stimuli-responsive materials

[1] B. Hötzer, I. L. Medintz, N. Hildebrandt, *Small* **2012**, *8*, 2297–2326.
[2] H. Wang, X. Ji, Z. A. Page, J. L. Sessler, *Mater. Chem. Front.* **2020**, *4*, 1024–1039.
[3] K. Nishiyama, M. Maeki, A. Ishida, H. Tani, H. Hisamoto, M. Tokeshi, *ACS Omega* **2021**, *6*, 8340–8345.
[4] H. Zhang, X. Hu, H. Zhu, L. Shen, C. Liu, X. Zhang, X. Gao, L. Li, Y. P. Zhu, Z. Li, *Front. Chem.* **2021**, *9*, 1–10.
[5] K. Mutoh, N. Miyashita, K. Arai, J. Abe, *J. Am. Chem. Soc.* **2019**, *141*, 5650–5654.
[6] C.-J. Zhong, X.-L. Hu, X.-L. Yang, H.-Q. Gan, K.-C. Yan, F.-T. Shu, P. Wei, T. Gong, P.-F. Luo, T. D. James, Z.-H. Chen, Y.-J. Zheng, X.-P. He, Z.-F. Xia, *ACS Appl. Mater. Interfaces* **2022**, *14*, 39808–39818.
[7] P. Hornbeck, *Curr. Protoc. Immunol.* **1992**, *1*, 2.1.1–2.1.22.
[8] A. A. Awasthi, P. K. Singh, *J. Phys. Chem. B* **2017**, *121*, 6208–6219.

[9] Y. Li, R. Xie, X. Pang, Z. Zhou, H. Xu, B. Gu, C. Wu, H. Li, Y. Zhang, *Talanta* **2019**, *205*, 120143.
[10] X. Cai, B. Liu, *Angew. Chem. Int. Ed.* **2020**, *59*, 9868–9886; *Angew. Chem.* **2020**, *132*, 9952–9970.
[11] R. V. Balaj, L. D. Zarzar, *Chem. Phys. Rev.* **2020**, *1*, 011301.
[12] L. D. Zarzar, V. Sresht, E. M. Sletten, J. A. Kalow, D. Blankschtein, T. M. Swager, *Nature* **2015**, *518*, 520–524.
[13] S. Djalali, B. D. Frank, L. Zeininger, *Soft Matter* **2020**, *16*, 10419–10424.
[14] A. E. Goodling, S. Nagelberg, B. Kaehr, C. H. Meredith, S. I. Cheon, A. P. Saunders, M. Kolle, L. D. Zarzar, *Nature* **2019**, *566*, 523–527.
[15] P. S. Marqués, B. D. Frank, A. Savateev, L. Zeininger, *Adv. Opt. Mater.* **2021**, *9*, 2101139.
[16] L. Zeininger, E. Weyandt, S. Savagatrup, K. S. Harvey, Q. Zhang, Y. Zhao, T. M. Swager, *Lab Chip* **2019**, *19*, 1327–1331.
[17] B. D. Frank, M. Antonietti, L. Zeininger, *Macromolecules* **2021**, *54*, 981–987.
[18] Y. Guo, Y. Fang, K. Jia, Y. Yu, L. Yu, H. Li, J. Zhang, X. Zheng, L. Huang, W. Wen, Y. Mai, *Macromol. Rapid Commun.* **2021**, *42*, 2100085.
[19] B. D. Frank, M. Perovic, S. Djalali, M. Antonietti, M. Oschatz, L. Zeininger, *ACS Appl. Mater. Interfaces* **2021**, *13*, 32510–32519.
[20] J. Li, A. Concellón, K. Yoshinaga, Z. Nelson, Q. He, T. M. Swager, *ACS Cent. Sci.* **2021**, *7*, 1166–1175.
[21] V. Trinh, C. S. Malloy, T. J. Durkin, A. Gadh, S. Savagatrup, *ACS Sens.* **2022**, *7*, 1514–1523.
[22] L. Zeininger, S. Nagelberg, K. S. Harvey, S. Savagatrup, M. B. Herbert, K. Yoshinaga, J. A. Capobianco, M. Kolle, T. M. Swager, *ACS Cent. Sci.* **2019**, *5*, 789–795.
[23] S. Djalali, P. Simón Marqués, B. D. Frank, L. Zeininger, *Adv. Funct. Mater.* **2021**, *32*, 2107688.
[24] M. Pavlovic, H. K. R. R. Babu, S. Djalali, M. Vranes, V. Radonic, L. Zeininger, *Anal. Chem.* **2021**, *93*, 9390–9396.
[25] B. D. Frank, S. Djalali, A. W. Baryzewska, P. Giusto, P. H. Seeberger, L. Zeininger, *Nat. Commun.* **2022**, *13*, 2562.
[26] A. Concellón, D. Fong, T. M. Swager, *J. Am. Chem. Soc.* **2021**, *143*, 9177–9182.
[27] L. D. Zarzar, J. A. Kalow, X. He, J. J. Walish, T. M. Swager, *Proc. Nat. Acad. Sci.* **2017**, *114*, 3821–3825.
[28] S. Savagatrup, D. Ma, H. Zhong, K. S. Harvey, L. C. Kimerling, A. M. Agarwal, T. M. Swager, *ACS Sens.* **2020**, *5*, 1996–2002.
[29] Z. Yang, Z. Chi, Z. Mao, Y. Zhang, S. Liu, J. Zhao, M. P. Aldred, Z. Chi, *Mater. Chem. Front.* **2018**, *2*, 861–890.
[30] J. Rouillon, C. Monnereau, C. Andraud, *Chem. Eur. J.* **2021**, *27*, 8003–8007.
[31] M. Gao, B. Z. Tang, *ACS Sens.* **2017**, *2*, 1382–1399.
[32] I. H. Lee, W. Song, J. Y. Lee, *Org. Electron.* **2016**, *29*, 22–26.
[33] W. Guan, W. Zhou, C. Lu, B. Z. Tang, *Angew. Chem. Int. Ed.* **2015**, *54*, 15160–15164; *Angew. Chem.* **2015**, *127*, 15375–15379.
[34] W. Guan, S. Wang, C. Lu, B. Zhong Tang, *Nat. Commun.* **2016**, *7*, 11811.
[35] J. T. Davies, E. K. Rideal, *Interfacial Phenomena*, Academic Press, New York, **1961**.

Manuscript received: December 5, 2022
Accepted manuscript online: January 20, 2023
Version of record online: February 22, 2023